Gamow-Teller transitions and magnetic properties of nuclei and shell evolution

Toshio Suzuki*
Department of Physics, College of Humanities and Sciences, Nihon University, Sakurajosui 3-25-40, Setagaya-ku, Tokyo 156, Japan

Rintaro Fujimoto
Department of Physics, University of Tokyo, Hongo, Bunkyo-ku, Tokyo 113-0033, Japan

Takaharu Otsuka
Department of Physics and Center for Nuclear Study, University of Tokyo, Hongo, Bunkyo-ku, Tokyo 113-0033, Japan
and RIKEN, Hirosawa, Wako-shi, Saitama 351-0198, Japan
(Received 13 September 2002; published 18 April 2003)

New aspects of quenching of Gamow-Teller (GT) transitions and magnetic moments are investigated for *p*-shell nuclei using an improved shell-model Hamiltonian with enhanced spin-flip proton-neutron interaction and modified single-particle energies. The present shell-model Hamiltonian thus obtained is used in the configuration space up to $(2-3)\hbar\omega$ excitations, and GT transitions and magnetic moments are calculated with bare *g* factors and bare axial-vector coupling constant. Manifestation of variable quenching due to changing gap between $0p_{3/2}$ and $0p_{1/2}$ is presented in GT transitions such as $^{12}\mathrm{C}\rightarrow{}^{12}\mathrm{N}$, $^{11}\mathrm{B}\rightarrow{}^{11}\mathrm{Be}$, and $^{9}\mathrm{Li}\rightarrow{}^{9}\mathrm{Be}$. A similar effect is shown for magnetic moments. Better agreement with experimental values is obtained systematically by using the present Hamiltonian for GT transitions and magnetic moments in most of *p*-shell nuclei, as well as for energy levels. Thus, the shell structure is changing from nucleus to nucleus in an orderly way (i.e., shell evolution), the inclusion of which leads us to an improved description of the GT and magnetic properties. It is stressed that the anomalous shell structure of exotic nuclei and the GT/magnetic properties of stable and exotic nuclei are linked through the same underlying mechanism.

DOI: 10.1103/PhysRevC.67.044302 PACS number(s): 21.10.Ky, 21.30.Fe, 21.60.Cs, 27.20.+n

I. INTRODUCTION

The nuclear structure is dominated by the shell structure, i.e., magic numbers. The spherical magic numbers have been presented for stable nuclei since the work of Mayer and coworkers [1]. Recently, however, the possible disappearance of some of these magic numbers and the appearance of new magic numbers have been suggested for some exotic nuclei as an effect of the spin-isospin component of the effective nucleon-nucleon (N-N) interaction in nuclei [2]. Various observed phenomena, as we shall see in detail in subsequent sections, can be explained in terms of the variation of the shell gap due to this interaction, with the disappearance of magic numbers 8 and 20 and the appearance of new magic numbers 6, 16, and 34 in some of exotic nuclei [2]. Thus, such changes of shell structure and related consequences can be studied in terms of the shell evolution paradigm [3]. In the case of *p*-shell nuclei, in particular, the effective N-N interaction has been modified in Ref. [2] in order to incorporate the spin-isospin property of a microscopic interaction based on the *G*-matrix formalism [4], providing a unified description of stable and exotic nuclei.

The spin-isospin component of the N-N interaction is known to have direct relevance to spin-isospin properties such as magnetic moments, Gamow-Teller (GT) transitions, etc. This relevance should be present both in stable and exotic nuclei. It is therefore of much interest what spin-isospin properties can be obtained from the effective N-N interactions that produce new magic numbers and annihilate some of the existing magic numbers in certain nuclei. In this paper, we shall carry out such a study by taking *p*-shell nuclei, thus providing a test of the shell evolution paradigm [3].

The magnetic moments and GT transitions have been studied extensively over decades for various nuclei. Theoretical studies include those for LS closed core ± 1 nucleon [5,6], *p*-shell nuclei [7], sd-shell nuclei [8], etc. A compilation of observed magnetic moments has been presented in Ref. [9], while GT transitions have been studied experimentally for *p*-shell nuclei as reported, for instance, in Ref. [10] for ^{12}C, in Ref. [11] for ^{11}Be, and in Refs. [12–14] for ^{11}Li. All these experimental data are discussed in this paper. The present study is made in a manner basically similar to the above theoretical works, while particular attention will be paid to modifications of effective N-N interactions mainly in their spin-isospin couplings and to new aspects emerging from such modifications.

As mentioned above, the effective interaction in the *p* shell has been modified in Ref. [2] from the Cohen-Kurath (CK) Hamiltonian [7]. It has been suggested in Ref. [2] that, for magic numbers of exotic nuclei, the proton-neutron (p-n) monopole interaction between two orbits $j_> = \ell + \frac{1}{2}$ and $j_< = \ell - \frac{1}{2}$ plays an important role. This monopole interaction is attractive, but its effects on the neutron (ν) $j_<$ orbit become weaker as the occupation of the proton (π) $j_>$ orbit decreases. This can be the case in certain neutron-rich nuclei, leading to a larger energy gap between $j_>$ and $j_<$ orbits created by the spin-orbit splitting. The same thing can be expressed the other way round: the original spin-orbit splitting for neutrons can be reduced effectively if a sufficiently large number of protons occupy the relevant $j_>$ orbit [2]. In the paradigm of the shell evolution, this is the mechanism, in

*Email address: suzuki@chs.nihon-u.ac.jp

the case of $\ell=2$, for the vanishing of the magicity at $N=20$ and the appearance of the magicity at $N=16$. The same mechanism leads to the vanishing of the magicity at $N=8$ and the appearance of a new magic number at $N=6$ for the case of $\ell=1$.

This $j_>$ and $j_<$ monopole interaction for the $0p_{3/2}$ and $0p_{1/2}$ combination was found to be rather weak in the CK Hamiltonian [7] in comparison with the microscopic interaction based on the *G*-matrix formalism [4]. Hence, its strength in the $T=0$ channel was made more attractive in Ref. [2] by the amount

$$\Delta\langle 0p_{3/2}0p_{1/2};J,T|V|0p_{3/2}0p_{1/2};J,T\rangle = V_M^T, \qquad (1)$$

where V_M^T stands for a constant independent of J. A J-independent V_M means a monopole shift. The value of V_M^T was taken to be -2 MeV for $T=0$, i.e, more attractive by 2 MeV for $T=0$ in Ref. [2]. Note that no modification was made for $T=1$ in Ref. [2] because of no apparent need. At the same time, the single-particle energy difference between the $0p_{3/2}$ and $0p_{1/2}$ orbits was modified by

$$\Delta\varepsilon_p \equiv \epsilon(0p_{1/2}) - \epsilon(0p_{3/2}), \qquad (2)$$

where $\epsilon(0p_{3/2}$ or $0p_{1/2})$ means a bare single-particle energy with respect to the ^{4}He inert core of the shell-model calculation. In the CK Hamiltonian, $\Delta\varepsilon_p$ is 0.14 MeV, while it was modified to be 3.85 MeV in Ref. [2]. Note that the latter value was estimated from observed levels of ^{5}He [2]. A similar value of $\Delta\varepsilon_p=3.99$ MeV or 4.0 MeV was adopted in Refs. [15] and [16], respectively.

The PSDMK2 Hamiltonian has been used sometimes for *p*-shell nuclei with the $p+sd$ shell configuration space [17–19]. Its *p*-shell part is the CK Hamiltonian [CK (8–16)] with slightly different single-particle energies resulting in $\Delta\varepsilon_p=0.3$ MeV [7]. Its $\langle p,sd|V|p,sd\rangle$ part is taken from the Millener-Kurath (MK) Hamiltonian [20], while its $\langle p^2|V|(sd)^2\rangle$ and $\langle (sd)^2|V|(sd)^2\rangle$ parts are from Kuo's *G*-matrix calculation [21,22]. The PSDMK2 Hamiltonian is very similar to the PSDMK Hamiltonian, while both are in the OXBASH package [22]. In the PSDMK, the CK-POT version is used for the CK [7].

A revised Hamiltonian has recently been introduced in Ref. [2], as referred to as OFU*. Its *p*-shell part is basically the same as the CK (8–16) Hamiltonian but it also includes the modifications mentioned above: $V_M^{T=0}=-2$ MeV in Eq. (1) and $\Delta\varepsilon_p=3.85$ MeV in Eq. (2). With this OFU* Hamiltonian, the parity inversion in the low-lying energy levels in ^{9}He and ^{11}Be is reproduced, while energy levels in ^{13}C remain almost unchanged [2]. This happens because the effect of $\Delta\varepsilon_p$ and that of $V_M^{T=0}$ cancel each other in stable nuclei, whereas the effect of the $j_>$-$j_<$ interaction becomes very weak in those exotic nuclei. Thus, this modification is in the line of the shell evolution paradigm [3].

One of new aspects expected from this modified Hamiltonian is a different quenching in spin-dependent transitions. As the energy gap between the $0p_{1/2}$ and $0p_{3/2}$ orbits becomes larger than that in the original CK Hamiltonian, the intermediate coupling nature characteristic to the CK Hamiltonian [7] may be weakened and the spin-dependent transitions can become more single-particle-like with larger strength, i.e., weaker quenching, particularly in certain exotic nuclei.

In the present paper, we study GT transitions and magnetic moments in *p*-shell nuclei with modified shell-model Hamiltonians. Here, we take a configuration space up to $2\hbar\omega$ or $3\hbar\omega$ excitations so as to take into account more explicitly the quenching effects due to the next higher shell in the spin-isospin modes. We then revise the shell-model Hamiltonian for the use in the $(2-3)\hbar\omega$ configuration space. Because the configuration mixing up to $2\hbar\omega$ excitations is usually good enough, a magnetic operator with the bare *g* factors and a GT operator with the bare axial-vector coupling constant can be used with such a truncation.

In the following section, we will mention how the shell-model Hamiltonian is modified in the present study and examine energy levels for some *p*-shell nuclei. We discuss effects of such modifications on GT transitions in Sec. III by taking an example of ^{12}C. The GT transitions in ^{11}B and ^{9}Li are investigated in Sec. IV, where we will find large effects of the variation of the $0p_{3/2}$-$0p_{1/2}$ gap. The magnetic moment is discussed in Sec. V with an example of ^{12}N. In Sec. VI, $B(GT)$ values of GT transitions and magnetic moments are studied in *p*-shell nuclei for which experimental data are available. As examples of typical features of exotic nuclei, the structure and magnetic moment of ^{11}Be are presented in Sec. VII, while two $N=8$ isotones, ^{11}Li and ^{12}Be, are discussed in Sec. VIII. A summary is given in Sec. IX.

II. HAMILTONIAN AND ENERGY LEVELS

The Hamiltonian to be used in the present study is basically the same as the OFU* Hamiltonian. However, since the present Hamiltonian is used with the inclusion of up to $(2-3)\hbar\omega$ configurations, we have to refit parameters of the Hamiltonian, because the OFU* Hamiltonian is for the $(0-1)\hbar\omega$ configuration space.

When the configuration space is expanded, one usually should modify the two-body effective interaction, because the effective interaction contains renormalization effects from other shells. In the present case, this modification is made empirically by rescaling some of two-body matrix elements: the matrix elements of the type $\langle 0p^2|V|0p^2\rangle$ are reduced by a factor 0.93, while those of the type $\langle 0p^2|V|(1s0d)^2\rangle$ are multiplied by a factor 0.75. This rescaling effect was found to be important to reproduce energy spectra of stable nuclei around ^{16}O [23], and appear to work in other nuclei as we shall see. For brevity, the $(0-1)\hbar\omega$ $[(2-3)\hbar\omega]$ space will be simply denoted the $0\hbar\omega$ $(2\hbar\omega)$ space hereafter.

A comparison of calculated levels in the $2\hbar\omega$ space to experimental levels leads us to the energy gap $\Delta\varepsilon_p=3.92$ MeV and the monopole correction $V_M^{T=0}=-2.14$ MeV. These new values of $\Delta\varepsilon_p$ and $V_M^{T=0}$ are very close to what have been done in Ref. [2]. Thus, the Hamiltonian of the present study is fixed as referred to as ''present.'' The single-particle wave functions of the usual harmonic oscillator potential are used.

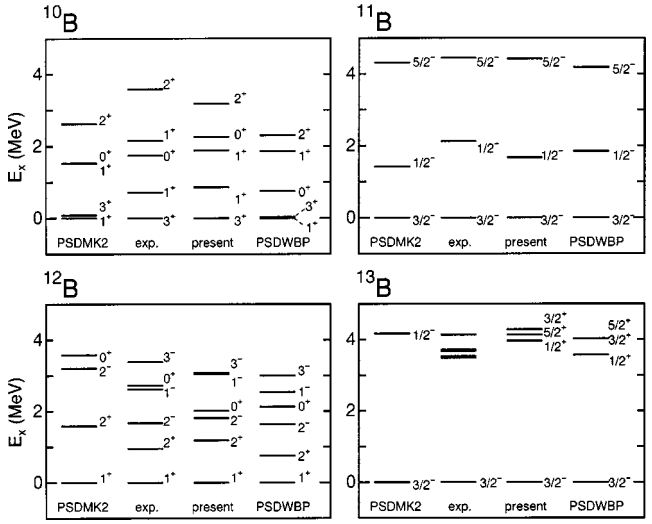

FIG. 1. Comparison of calculated and experimental energy levels for $^{10-13}$B isotopes. Calculated energy levels are obtained for the PSDMK2, and the present and the PSDWBP Hamiltonians.

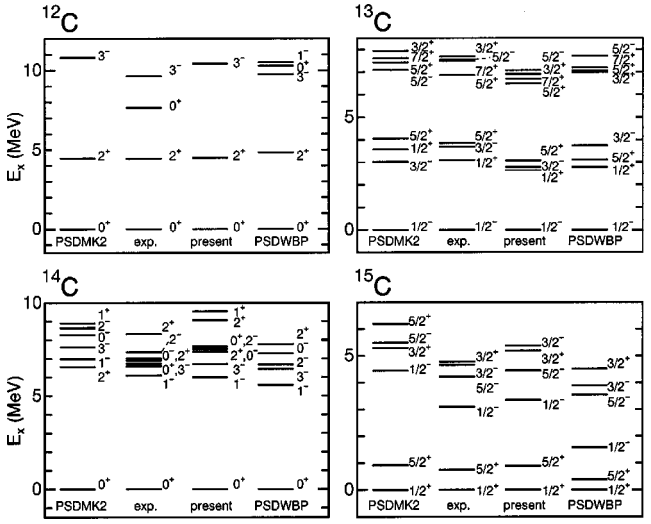

FIG. 2. Comparison of calculated and experimental energy levels for $^{12-15}$C isotopes. Calculated energy levels are obtained for the PSDMK2, and present and the PSDWBP Hamiltonians.

We now show energy levels of B and C isotopes, as examples, in order to examine to what extent the levels are reproduced. The B and C isotopes are quite relevant because there are three or four protons, respectively, in $0p_{3/2}$ in the filling configuration. We will show levels of ^{11,12}Be in Secs. VII and VIII.

Figure 1 shows calculated energy levels of B isotopes for mass numbers $A=10$ (i.e., $N=Z)\sim 13$, in comparison to experimental ones. Energy levels are calculated by using the PSDMK2 or the present Hamiltonian including up to $(2-3)\hbar\omega$ excitations. A set of Warburton-Brown Hamiltonian (WBP) [26] is also used including up to $(0-1)\hbar\omega$ excitations within the p-sd–shell space (this Hamiltonian will be referred to as PSDWBP). The present Hamiltonian reproduces well the experimental energy levels. Although the other Hamiltonians can reproduce experimental levels to a similar extent in most of the cases, some differences are seen in ^{10,12}B. The ground state of ^{10}B is a 3^+ state in the experiment. This can be reproduced precisely with the present Hamiltonian, whereas the PSDMK2 and PSDWBP produce a 1^+ ground state. The lowest 1^+ state is nearly 1 MeV high both in experiment and in the present. The present Hamiltonian locates this 1^+ state at a correct height, partly because the $0p_{1/2}$ orbit is well above $0p_{3/2}$.

We show in Fig. 2 calculated energy levels of C isotopes for mass numbers $A=12$ (i.e., $N=Z)\sim 15$, in comparison to experimental ones. One finds that the three Hamiltonians reproduce experimental levels to a similar extent. In C isotopes, the proton $0p_{3/2}$ orbit is substantially occupied. This means that the neutron $0p_{1/2}$ orbit is pulled down by the strong $j_>$-$j_<$ p-n monopole attraction in the case of the present Hamiltonian. In other words, the effective location of $0p_{1/2}$ does not differ too much among the three Hamiltonians. The three Hamiltonians can reproduce not only positive-parity levels but also negative-parity levels. On the other hand, towards ^{15}C, the neutron effective p-sd–shell gap may remain too large in the PSDMK2.

We briefly discuss energy levels of ^{15}O (^{15}N) shown in Fig. 3. As compared to the PSDMK2 calculation, if we increase only $\Delta\varepsilon_p$ by 3.55 MeV, the spacing between the first $1/2^-$ and $3/2^-$ levels becomes wider to a value $\sim$10 MeV. Note that this spacing is related to the LS splitting of the $0p_{1/2}$ and $0p_{3/2}$ orbits, and indeed the LS splitting between their hole states in the $0\hbar\omega$ model space. We then include $V_M^{T=0}=-2$ MeV, decreasing the spacing to 8.01 MeV. The expansion of the model space and the associated renormalization of the interaction further reduce the spacing by 0.63 MeV and 0.50 MeV, respectively, resulting in the spacing of 6.88 MeV, which is rather close to the experimental value of 6.18 MeV in ^{15}O and 6.32 MeV in ^{15}N. We thus confirm that the LS splitting should be treated reasonably well also towards the end of the p shell. Positive-parity states are described by the present Hamiltonian somewhat too high (while better than PSDMK2 result) due to insufficient improvement in the sd-shell-related sector of the Hamiltonian as discussed later.

The agreement with experiment in Figs. 1–3 seems to suggest that the present Hamiltonian can handle excitations

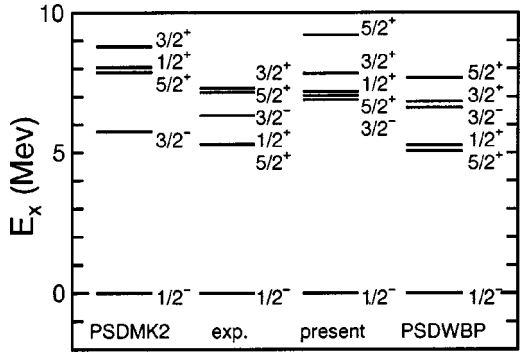

FIG. 3. Comparison of calculated and experimental energy levels for ^{15}O. Calculated energy levels are obtained for the PSDMK2, and present and the PSDWBP Hamiltonians.

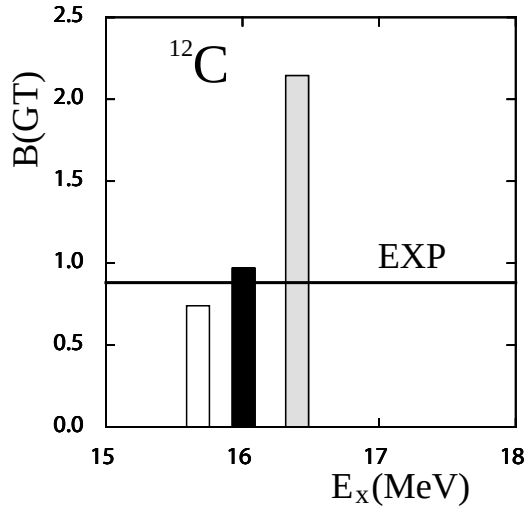

FIG. 4. Effect of the modification of the single-particle energies on the GT transition $^{12}\mathrm{C}\rightarrow{}^{12}\mathrm{N}\ (1^+_{\mathrm{g.s.}})$. White histogram denotes the calculated result for the GT transition by the PSDMK2 Hamiltonian. The shaded histogram includes the effect of the modification of the single-particle energies [52]. The black one corresponds to the result of the present Hamiltonian. The experimental data [10] are indicated by the solid horizontal line labeled by "EXP."

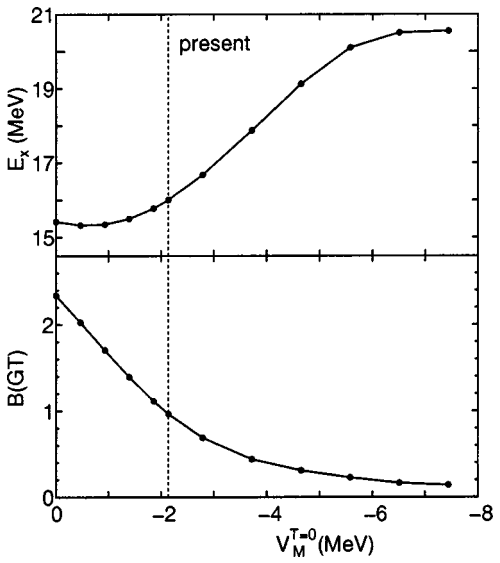

FIG. 5. Excitation energy and $B(GT)$ value as a function of $V_M^{T=0}$ in Eq. (1) [52]. The value of $V_M^{T=0}$ in the present Hamiltonian is indicated by dashed lines.

from the p shell to the sd shell to the extent needed for the description of quenching effects due to the two-particle–two-hole excitations.

III. GAMOW-TELLER TRANSITIONS

We now investigate GT transitions in terms of the $B(GT)$ value, which is written as

$$B(GT)=\frac{1}{2J_i+1}|\langle J_f\|\sigma\tau_{\pm}\|J_i\rangle|^2, \tag{3}$$

where J_i (J_f) denotes the angular momentum of the initial (final) state, and $\sigma(\tau)$ denotes the spin (isospin) operator with the convention $\tau_-|\pi\rangle=|\nu\rangle$.

We first show the effect due to $\Delta\varepsilon_p$ in Eq. (2) on the GT transition. Figure 4 shows this effect in the $^{12}\mathrm{C}\rightarrow{}^{12}\mathrm{N}\ (1^+_{\mathrm{g.s.}})$ transition. We start with the PSDMK2 Hamiltonian, of which the currently relevant part is the CK Hamiltonian [7]. The GT transition to the $1^+_{\mathrm{g.s.}}$ state is shown in Fig. 4 by the white histogram. We then change $\Delta\varepsilon_p$ from 0.3 MeV to 3.92 MeV, as described in Sec. II. The GT transition is shown by the shaded histogram in Fig. 4, which is enhanced from the CK value by about a factor of 3. The excitation energy from the ^{12}C ground state is pushed up too. It is clear that the single-particle aspect becomes dominant. The $B(GT)$ value and excitation energy by the present Hamiltonian is exhibited in Fig. 4 by the black histogram, which is in between. Figure 4 includes the experimental $B(GT)$ value, which has been obtained from the formula

$$ft=\frac{6147}{(g_A/g_V)^2B(GT)}, \tag{4}$$

where a constant value of 6147 is taken from Ref. [24]. In Eq. (4), g_A and g_V are the axial-vector and vector coupling constants, respectively; and a bare axial-vector coupling constant $g_A/g_V=-1.26$ for the β decay is assumed [25]. The result of the present Hamiltonian is actually in a good agreement with this experimental value. We now show how the $B(GT)$ value is reduced by $V_M^{T=0}$ in Eq. (1).

In order to see the effect of $V_M^{T=0}$, we vary the value of $V_M^{T=0}$ from 0 to some large negative value. Since the 1^+ ground state of ^{12}N is in the same isospin multiplet as an excited 1^+ state of ^{12}C, we discuss the excitation energy of this 1^+ state of ^{12}C instead of Q_β of the ^{12}N ground state. The excitation energy of this 1^+ state of ^{12}C is shown in Fig. 5 as a function of $V_M^{T=0}$. In the lower part of the same figure, its $B(GT)$ value is exhibited. Note that $\Delta\varepsilon_p$ is kept to its present value, 3.92 MeV.

The structure near $V_M^{T=0}=0$ is still that of the single-particle model with large $B(GT)$ value. Figure 5 indicates how this single-particle situation is destroyed as $V_M^{T=0}$ is driven from 0 to large negative values.

The final state of GT transition, i.e., the first 1^+ state of ^{12}N, contains about one proton and almost no neutron in $0p_{1/2}$ for $0>V_M^{T=0}>-4$ MeV. This state is connected by the GT transition from the j-j coupling limit configuration of the ^{12}C ground state, i.e., $\pi 0p_{3/2}^4$ and $\nu 0p_{3/2}^4$. Although this process produces large $B(GT)$ values, this configuration becomes less dominant as $V_M^{T=0}$ becomes more negative. This happens because, as $V_M^{T=0}$ becomes a larger negative number, another excited configuration $\pi 0p_{1/2}^1\ 0p_{3/2}^3\times\nu 0p_{1/2}^1\ 0p_{3/2}^3$ becomes more favored in energy and becomes more mixed in the ^{12}C ground state, owing to the attraction between $\pi\ 0p_{3/2}$ and $\nu\ 0p_{1/2}$, or vice versa. Such decreasing probability of the j-j coupling limit configuration is the basic reason for the monotonic decrease of the $B(GT)$ value in Fig. 5. In addition, this mixed configuration is connected by

the GT transition to the above configuration of the first 1^+ state of ^{12}N with the opposite sign. While the magnitude is much less from this process, this destructive interference makes $B(GT)$ even smaller. Thus, the $B(GT)$ value in Fig. 5 decreases so rapidly as $V_M^{T=0}$ becomes more negative, and approaches even less than 10% for $V_M^{T=0}<-6$ MeV. This region of $V_M^{T=0}$ with large negative value approaches the LS coupling limit [27].

We next discuss the excitation energy of the 1^+ ground state of ^{12}N from the ^{12}C ground state. When $V_M^{T=0}$ starts to move to a negative value, the neutron $0p_{1/2}$ orbit is pulled down by protons in $0p_{3/2}$, and the excitation energy is lowered slightly. The excitation energy then starts to increase for larger magnitude of $V_M^{T=0}$. The excited configuration, $\pi 0p_{1/2}^1\ 0p_{3/2}^3 \times \nu\ 0p_{1/2}^1\ 0p_{3/2}^3$, is more mixed in the ^{12}C ground state, pulling its own energy down but the excitation energies of other states up. Only after around $V_M^{T=0}=-4$ MeV, an excited configuration $\pi 0p_{1/2}^1\ 0p_{3/2}^4 \times \nu\ 0p_{1/2}^2\ 0p_{3/2}^1$, begins to be mixed in the ^{12}N state, making the excitation energy almost constant but keeping $B(GT)$ further down.

Summarizing the above discussions, one can explain how the excitation energy and $B(GT)$ value are affected by $\Delta\varepsilon_p$ in Eq. (2) and $V_M^{T=0}$ in Eq. (1). Figure 5 includes the results of the present Hamiltonian, which are in reasonable agreement with experiment [10]. It seems that the right combination of $\Delta\varepsilon_p$ and $V_M^{T=0}$ is contained in the present Hamiltonian, while they are not adjusted to any GT properties.

The $V_M^{T=0}$ term is related to the $\tau\tau$-$\sigma\sigma$ interaction as discussed in [2,3]. A stronger attraction in $V_M^{T=0}$ corresponds to a larger positive strength of the $\tau\tau$-$\sigma\sigma$ interaction. As this strength becomes larger, in general, the sum-rule state of the operator $\tau\sigma$ is pushed up in energy. On the other side, the ground state is changed so as to make its $B(GT)$ sum rule smaller, because the $B(GT)$ sum rule and the expectation value of the $\tau\tau$-$\sigma\sigma$ term are proportional including the sign. Namely, the larger $B(GT)$, the higher energy (less binding) for the ground state. Note that the $\tau\tau$-$\sigma\sigma$ interaction with the positive sign acts as an attraction for the $j_>$-$j_<$ monopole interaction because the exchange process matters as stressed in Ref. [2]. Although the $V_M^{T=0}$ term is not precisely like the $\tau\tau$-$\sigma\sigma$ interaction, it contains the above general properties rather well. In this view, the general and global trend in Fig. 5 can be interpreted. When the absolute magnitude of $V_M^{T=0}$ is small, contibutions other than $\tau\tau$-$\sigma\sigma$ component such as vector components (two-body spin-orbit as well as the antisymmetric spin-orbit terms) may be sizable. The contribution of the LS vector term turns out to be 12% and 6% of the total $T=0$ $p_{3/2}$-$p_{1/2}$ monopole matrix element for $V_M^{T=0}=0$ MeV and -1 MeV, respectively. Therefore, in the region at $V_M^{T=0}\sim 0$ MeV, the reduction of the $B(GT)$ value can be connected with the reduction of the vector component of the interaction. Details of such effects are discussed in Ref. [28]. On the other hand, if $V_M^{T=0}<-1$ MeV, the LS vector term plays rather minor role and the structure becomes dominated by the $\tau\tau$-$\sigma\sigma$ interaction.

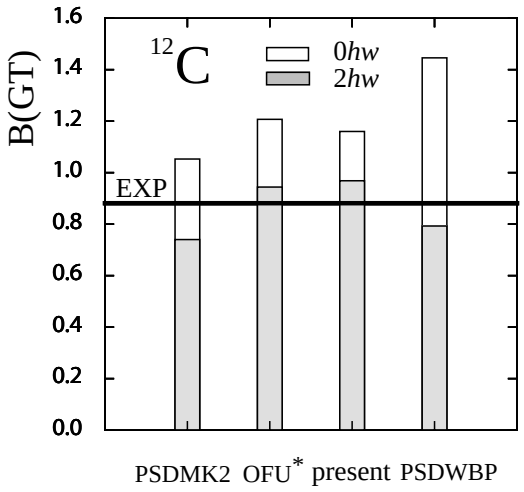

FIG. 6. $B(GT)$ values for the transition $^{12}\mathrm{C}\rightarrow{}^{12}\mathrm{N}$ $(1^+_{\mathrm{g.s.}})$. They are obtained by the shell-model calculations within $0p$-$1s0d$ shells including up to $0\hbar\omega$ (white bars) and $2\hbar\omega$ (dashed bars) excitations with the use of the PSDMK2, OFU*, and present and PSDWBP Hamiltonians. Experimental value ''EXP'' is taken from [10].

Figure 6 shows calculated $B(GT)$ values for the transition $^{12}\mathrm{C}\rightarrow{}^{12}\mathrm{N}$ $(1^+,\ T=1)$, where shell-model calculations are performed with various Hamiltonians such as PSDMK2, PSDWBP [26], OFU*, and present. The shell-model configuration space is taken up to $0\hbar\omega$ and $2\hbar\omega$. Note that the PSDWBP and OFU* Hamiltonians are designed for the $0\hbar\omega$ space, whereas the others are for the $2\hbar\omega$ space. One finds empirically that the OFU* Hamiltonian with the $0\hbar\omega$ space needs a quenching factor $g_A^{eff}/g_A\sim 0.86$ to reproduce the experimental value.

In contrast, since the PSDMK2 and present Hamiltonian in the $2\hbar\omega$ space include two-particle–two-hole ($2p$-$2h$) excitations, there should be no quenching factor due to $2p$-$2h$ excitations with them. Indeed, both Hamiltonians can reproduce the experimental value within about 15% or 10%, respectively. The $B(GT)$ value is larger by about 30% for the present Hamiltonian than the value for the PSDMK2. We can see clearly that, even for ^{12}C, the single-particle aspect is stronger in the present Hamiltonian than in the CK, although the energy levels look alike between the two. The occupation number of $0p_{1/2}$ ($0p_{3/2}$) orbit in the ground state of ^{12}C is 1.570 (6.220) for the PSDMK2, but changes to 1.442 (6.415) for the present Hamiltonian. We notice less mixing of the $0p_{1/2}$ and $0p_{3/2}$ orbits in the present Hamiltonian. The result obtained by the present Hamiltonian with the space up to $2\hbar\omega$ excitations is close to the observed value, that is, larger than the experimental one only by 9.3%. There are additional reductions induced by higher configurations as well as the Δ_{33}-isobar exchange current: the $B(GT)$ value is reduced by $\sim$5% due to the Δ_{33}-isobar exchange current [29] and by $\sim$4% by including the contributions from $4\hbar\omega$ configuration space. Namely, the combined reduction of $B(GT)$ is about 10%, which brings the result of the present Hamiltonian right on the experiment, whereas it pushes the PSDMK2 result further down. Note that the factor

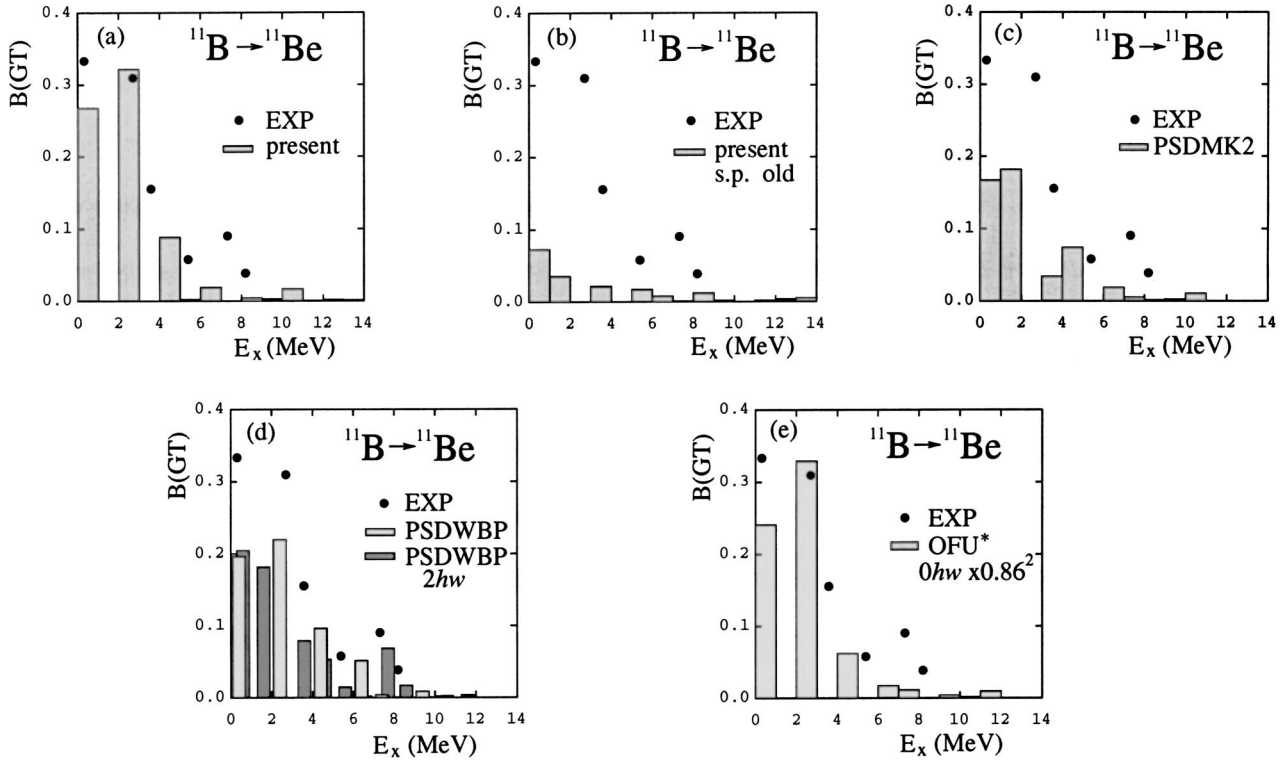

FIG. 7. (a) $B(GT)$ values for ^{11}B→^{11}Be ($1/2^-$, $3/2^-$, $5/2^-$). They are obtained by the shell-model calculations with the present Hamiltonian including up to $2\hbar\omega$ excitations. Experimental data are taken from Ref. [11]. (b) The same as in (a) except that $\Delta\varepsilon_p$ is not taken to be 3.85 MeV (value in the present Hamiltonian), but 0.3 MeV [20]. (c) The same as in (a) for the PSDMK2 Hamiltonian. (d) The same as in (a) for the PSDWBP Hamiltonian within $0\hbar\omega$ space with a quenching factor of $(0.78)^2=0.61$ (dashed), and those for the same Hamiltonian including up to $2\hbar\omega$ excitations. (e) The same as in (a) for the OFU* Hamiltonian within the $0\hbar\omega$ space with a quenching factor of $(0.86)^2$.

g_A^{eff}/g_A becomes about 0.95 due to the quenching by these two mechanisms combined.

In case of the PSDWBP Hamiltonian, the energy levels are fitted within the $0\hbar\omega$ space [26]. When we adopt the calculated result for the $B(GT)$ value within the $0\hbar\omega$ space, we need a quenching factor $g_A^{eff}/g_A=0.78$, a somewhat stronger quenching than that for the OFU*.

IV. GAMOW-TELLER TRANSITIONS IN ^{11}B AND ^{9}Li

In this section, we investigate GT transitions from ^{11}B and ^{9}Li as well as muon capture reaction on ^{11}B.

Calculated $B(GT)$ values are shown in Fig. 7 for ^{11}B →^{11}Be ($1/2^-$, $3/2^-$, $5/2^-$) transitions obtained by using the (a) present, (b) present with $\Delta\varepsilon_p$ small, (c) PSDMK2, (d) PSDWBP, and (e) OFU* Hamiltonians. The space is of $2\hbar\omega$ for (a)–(c), of 0 and $2\hbar\omega$ for (d), and of $0\hbar\omega$ for (e). The contributions of the Δ_{33}-isobar exchange current are evaluated [29] and included in the $B(GT)$ values for all $2\hbar\omega$-space calculations.

For the $0\hbar\omega$-space calculations by PSDWBP and OFU* Hamiltonians, the quenching factors 0.78 and 0.86, respectively, obtained in Sec. III are multiplied to the transition amplitude. The Δ_{33}-isobar exchange current effects are assumed to be included already in these quenching factors as a result of the fit, and are not explicitly evaluated.

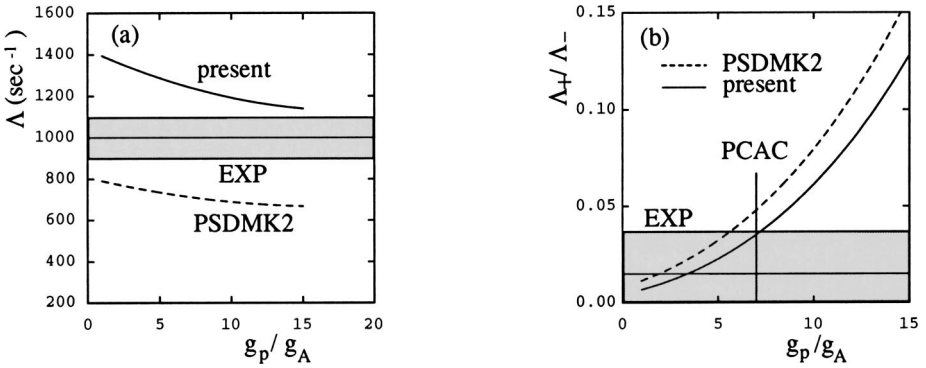

FIG. 8. (a) Averaged transition rates for ^{11}B (μ^-, ν_μ) ^{11}Be ($1/2^-$, 0.32 MeV) from the two hyperfine states $F=1$ and 2, calculated for the PSDMK2 and present Hamiltonians. (b) The ratio Λ_+/Λ_- of the transition rates from the two hyperfine states $F=2$ and 1 in ^{11}B are also shown for the PSDMK2 and present Hamiltonians. In (a) and (b), experimental values are indicated by hatched areas [32,33].

The $B(GT)$ values with the present Hamiltonian show alarge enhancement of (70±10)% (about 50%) over those with the PSDMK2 (PSDWBP) Hamiltonian at $E_x \leqslant 4$ MeV. The OFU* Hamiltonian also gives a similar enhancement. As we see from Fig. 7(b), this enhancement may be considered to stem from the more prominent single-particle nature in ^{11}B as a result of the shell evolution, which occurs more weakly with the CK (or PSDMK2) Hamiltonian. A recent measurement of these $B(GT)$ values by the (n,p) reaction [11] supports this enhancement of the $B(GT)$ values.

A similar enhancement is obtained in the muon capture reaction ^{11}B (μ,ν_μ) ^{11}Be $(1/2^-,\ 0.32$ MeV). Transition rates from the two hyperfine states in ^{11}B are calculated. The calculated statistically averaged transition rate $\Lambda = \frac{5}{8}\Lambda_+ + \frac{3}{8}\Lambda_-$, where Λ_+ and Λ_- are the transition rates from the two hyperfine states $F=2$ and 1, respectively, are shown in Fig. 8(a) as a function of g_p/g_A. Here, g_p and g_A stand for pseudoscalar and axial-vector coupling constants, respectively. The value of g_A is taken to be the bare one: $g_A/g_V = -1.26$. The rates Λ_+ and Λ_- are given by

$$\Lambda_+ = V\left(\frac{3}{2}\mu_1(2)^2 + \frac{1}{10}\mu_2(2)^2 + \frac{8}{5}\mu_2(-3)^2 - \sqrt{\frac{3}{5}}\mu_1(2)\mu_2(2)\right),$$

$$\Lambda_- = V\left(\frac{8}{3}\mu_1(-1)^2 + \frac{1}{6}\mu_1(2)^2 + \frac{5}{2}\mu_2(2)^2 + \sqrt{\frac{5}{3}}\mu_1(2)\mu_2(2)\right), \quad (5)$$

where $V = 4(\alpha Z m_\mu)^3 q^2\ [(2J_f+1)/(2J_i+1)]$, with J_i (J_f) being the spin of the initial (final) nuclear state. Here, $\mu_J(\kappa)$'s are matrix elements [30] with transferred angular momentum J; $|J_i - J_f| \leqslant J \leqslant J_i + J_f$, and κ denotes ν_μ states: $\kappa = -1$, 2, and -3 corresponds to $1s_{1/2}$, $1d_{3/2}$, and $1d_{5/2}$, respectively.

The rates obtained by the present Hamiltonian are enhanced by about 70–80 % compared to those by the PSDMK2 Hamiltonian [31], which were smaller than the observed value [32]. This underestimation by the PSDMK2 has remained a puzzle since enhancement instead of quenching has been needed to explain the experiment. Such enhancement is unlikely in the spin-isospin dependent transition. The experimental value of the rate, $\Lambda \sim 1000 \pm 100\ \mathrm{sec}^{-1}$ [32], is more consistent with the results of the present Hamiltonian as the new results suggest the necessity of the quenching effects.

The ratio of the transition rates, Λ_+/Λ_-, is also studied. Calculated results for the ratio are shown in Fig. 8(b). Smaller values for the ratio are obtained for the present Hamiltonian than for the PSDMK2. For a given value of the ratio Λ_+/Λ_-, g_p/g_A is shifted by about 1 by the present Hamiltonian compared to the PSDMK2, if g_p/g_A is around its PCAC value of 7. Up to now, experimental information on the ratio is not sufficient. An experiment gives 0.015 ±0.022 [33], while an old one gives an upper limit for the ratio, namely, ⩽0.26 [32]. The present Hamiltonian favors a value closer to the PCAC value than the PSDMK2. It would be quite interesting to carry out muon capture experiments to obtain a more accurate value of the ratio as well as those of the reaction rates.

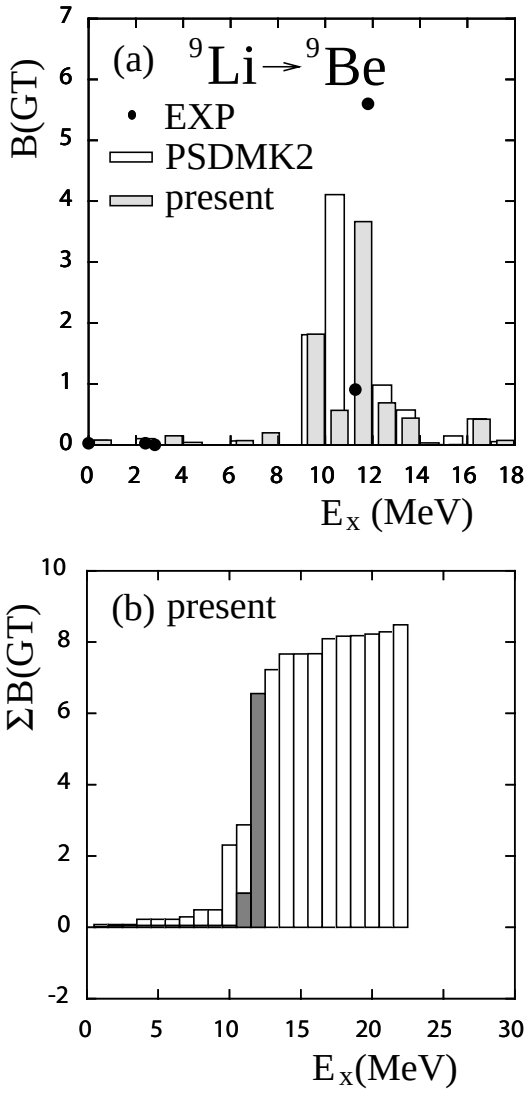

FIG. 9. (a) $B(GT)$ values for ^{9}Li→^{9}Be $(1/2^-,\ 3/2^-,\ 5/2^-)$. They are obtained by the shell-model calculations with the use of the present (hatched) and the PSDMK2 (blank) Hamiltonians including up to $2\hbar\omega$ excitations. Experimental values are taken from Ref. [34]. (b) Sum of the $B(GT)$ values for ^{9}Li→^{9}Be. White bars denote calculated values obtained by the present Hamiltonian while black bars represent experimental data (up to 12 MeV).

A remarkable improvement in the theoretical description can be seen also in the GT transitions ^{9}Li→^{9}Be $(1/2^-,\ 3/2^-,\ 5/2^-)$. The results are shown in Fig. 9. $B(GT)$ obtained for the present Hamiltonian is enhanced around $E_x = 11$–12 MeV region, and the strength is shifted toward higher excitation energy compared to the PSDMK2. Agreement with the experimental values [34] is considerably improved for the present Hamiltonian.

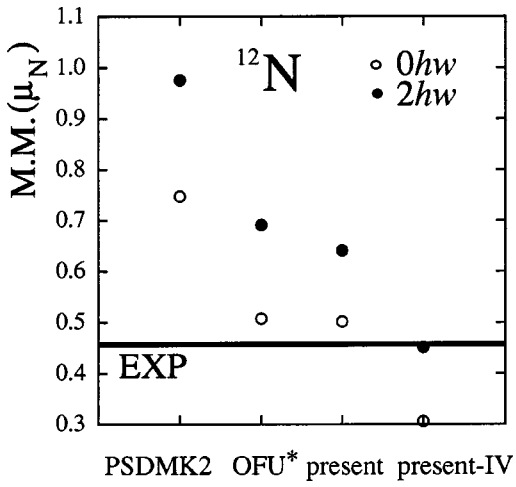

FIG. 10. Magnetic moment of the ground state of ^{12}N. Experimental value is taken from Refs. [35,36]. Calculated values are indicated by open ($0\hbar\omega$) and closed ($2\hbar\omega$) circles. The PSDMK2, and OFU* and present Hamiltonians are taken. The present-IV result includes the isovector correction to $g^{(\ell)}$'s.

V. MAGNETIC MOMENTS

We now turn to another major subject of this paper: magnetic moment. The magnetic moment operator is written as

$$\vec{\mu}=g_\pi^{(\ell)}\vec{\ell}_\pi+g_\nu^{(\ell)}\vec{\ell}_\nu+g_\pi^{(s)}\vec{s}_\pi+g_\nu^{(s)}\vec{s}_\nu, \tag{6}$$

where $\vec{\ell}$ and $\vec{s}$ stand for orbital and spin angular momenta, respectively, and the g's with superscripts ℓ and s denote similarly orbital and spin g factors. The shell-model calculations shown below are carried out basically in the $2\hbar\omega$ space. The bare spin g factors are, therefore, reasonable, and we use $g_\pi^{(s)}=5.59\mu_N$ and $g_\nu^{(s)}=-3.83\mu_N$ throughout this paper. The situation is slightly different for orbital contributions, because sizable isovector effects from meson exchange processes have been known [5,6]. Thus, in many cases discussed below, an isovector correction of $\delta g_{\pi,\nu}^{(\ell)}=\pm 0.15\mu_N$ is included, which means $g_\pi^{(\ell)}=1.15\mu_N$ and $g_\nu^{(\ell)}=-0.15\mu_N$. The results are then indicated by the label "IV." Note that $\delta g_{\pi,\nu}^{(\ell)}=\pm 0.15\mu_N$ is a commonly used value. For results without IV, the bare values $g_\pi^{(\ell)}=1\mu_N$ and $g_\nu^{(\ell)}=0\mu_N$ are employed.

Figure 10 shows the magnetic moment of the ground state of ^{12}N. Calculated values are obtained with PSDMK2, and OFU* and present Hamiltonians within the $0\hbar\omega$ and $2\hbar\omega$ spaces, while the first and the last are designed for the $2\hbar\omega$ space and the middle one for the $0\hbar\omega$ space.

In a naive picture, the magnetic moment of ^{12}N is the sum of the contributions of $\pi p_{1/2}$ and $\nu p_{3/2}$; $\mu=-g_\pi^{(\ell)}+\frac{1}{2}(g_\pi^{(s)}+g_\nu^{(s)})=-0.12\mu_N$. Due to the mixing of other configurations with the excitation from $p_{3/2}$ to $p_{1/2}$, the transition moment between these orbits affects the above value, enhancing the moment in this case. Since the PSDMK2 Hamiltonian causes this admixture to be too strong due to $p_{3/2}$ and $p_{1/2}$ single-particle energies being nearly degenerate, the calculated magnetic moment overshoots the experimental value. Note that the $0\hbar\omega$ value of PSDMK2 is nothing but the CK prediction. This deviation is remedied considerably in the result of the OFU* Hamiltonian, which produces reduced admixture of higher configurations. The present Hamiltonian gives us rather similar results to the OFU*. On the other hand, the $2\hbar\omega$ result is still too high without the isovector correction of the orbital contribution. In fact, once the corrected $g^{(\ell)}$'s are used, the calculation can reproduce the experiment quite well. Note that nothing has been adjusted to the measured magnetic moment.

Thus, one sees that the present Hamiltonian seems to be more suitable for the description of magnetic moment of p-shell nuclei owing to its modified spin-isospin and single-particle properties. This expectation is to be examined with other nuclei in the following section.

VI. SYSTEMATIC SURVEY OVER *p*-SHELL NUCLEI

We shall now test the predictions of the present Hamiltonian systematically. The calculated $B(GT)$ values for GT transitions and those of magnetic moments are summarized in Tables I and II, respectively, for p-shell nuclei with experimental data available [9,35–37]. Experimental $B(GT)$ values are derived from observed log ft values by using Eq. (4) with $g_A/g_V=-1.26$ [25]. The Fermi transition strength is subtracted from the denominator on the right-hand side of Eq. (4) if it exists. As we see from the tables, in most cases where the PSDMK2 Hamiltonian gives reasonable account of the experimental values, our modified (i.e., OFU* and present) Hamiltonians give generally better agreement with the observations, though the improvements are rather modest. In cases where substantial deviations are found between the PSDMK2 results and the experimental values, the modified Hamiltonians give remarkable improvements. Experimental values are reproduced better in most cases by the modified Hamiltonians, also as compared to the results of the PSDWBP and PSDWBT [37] Hamiltonians.

For GT transitions, improvements are minor, probably because they occur between nuclei closer to the β-stability line. The exceptions are ^{9}C and ^{9}Li. Here, one does not find much improvement. Since these are mirror nuclei, their log ft values should be equal in view of the isospin symmetry. The isospin symmetry, however, may be broken significantly because of loose binding. On the other hand, the experimental log ft values are still quite close to each other. It is an open question whether this is an anomaly or not. We shall come back to these cases when we discuss their magnetic moments. Among $B(GT)$ values, the largest improvement is found in the GT transition $^{14}\mathrm{C}\rightarrow{}^{14}\mathrm{N}\,(1^+_{\mathrm{g.s.}})$: the $B(GT)$ (log ft) value is decreased by a factor of 156 (increased by 2.2) when the present Hamiltonian is used instead of the PSDMK2 [35]. This is due to an improved cancellation among contributions from vector and tensor components of the interaction.

The agreement of the calculated magnetic moments with the experimental values is also improved, as expected from the preceding section. We notice that the isovector correction to the $g^{(\ell)}$'s improves the agreement in many cases or keeps the result nearly unchanged in most other cases.

Let us take ^{12}B-^{12}N mirror pair as an example. The mag-

TABLE I. Calculated and observed $B(GT)$ values in p-shell nuclei. Calculated values are obtained in the configuration space indicated on the second row. Calculated values for PSDWBT are taken from Ref. [37].

Transition $J_i^\pi T_i$, $J_f^\pi T_f$	Experiment	PSDMK2		OFU*	Present		PSDWBP	PSDWBT
Space		$0\hbar\omega$	$2\hbar\omega$	$0\hbar\omega$	$0\hbar\omega$	$2\hbar\omega$	$0\hbar\omega$	$0\hbar\omega$
^{6}He$\rightarrow^6$Li	4.763(12)	5.451	5.463	5.615	5.593	5.593	3.900	5.750
0^+1, 1^+0								
^{7}Be$\rightarrow^7$Li								
$\frac{3}{2}-\frac{1}{2}$, $\frac{3}{2}-\frac{1}{2}$	1.311(5)	1.613	1.614	1.519	1.509	1.509	1.638	1.589
$\frac{3}{2}-\frac{1}{2}$, $\frac{1}{2}-\frac{1}{2}$	1.132(8)	1.303	1.305	1.294	1.289	1.290	1.289	1.317
^{8}He$\rightarrow^8$Li	0.264(5)	0.3971	0.4665	0.3800	0.2921	0.3293	0.0297	0.2005
0^+1, 1^+1								
^{9}C$\rightarrow^9$B								
$\frac{3}{2}-\frac{3}{2}$, $\frac{3}{2}-\frac{1}{2}$	0.0206(37)	0.0842	0.0724	0.0886	0.0826	0.0757	0.0267	0.0514
$\frac{3}{2}-\frac{3}{2}$, $\frac{5}{2}-\frac{1}{2}$	0.0130(51)	0.0477	0.0542	0.0567	0.0529	0.0549	0.0108	0.0421
^{9}Li$\rightarrow^9$Be								
$\frac{3}{2}-\frac{3}{2}$, $\frac{3}{2}-\frac{1}{2}$	0.0190(11)	0.0842	0.0724	0.0886	0.0826	0.0757	0.0267	0.0514
$\frac{3}{2}-\frac{3}{2}$, $\frac{5}{2}-\frac{1}{2}$	0.0285(33)	0.0477	0.0542	0.0567	0.0529	0.0549	0.0108	0.0421
^{10}C$\rightarrow^{10}$B	3.467(8)	4.545	4.992	4.400	4.414	4.712	4.722	4.634
0^+1, 1^+0								
^{11}C$\rightarrow^{11}$B	0.3472(45)	0.5283	0.5391	0.5695	0.5927	0.5876	0.7880	0.6796
$\frac{3}{2}-\frac{1}{2}$, $\frac{3}{2}-\frac{1}{2}$								
^{11}Li$\rightarrow^{11}$Be	0.0086(24) [12–14]	0.0787	0.0654	0.1030	0.1030	0.0656	0.0850	0.0732
$\frac{3}{2}-\frac{5}{2}$, $\frac{1}{2}-\frac{3}{2}$								
^{12}B$\rightarrow^{12}$C								
1^+1, 0^+0	0.3288(15)	0.3508	0.2467	0.4024	0.3867	0.3228	0.4820	0.5064
1^+1, 2^+0	0.0298(10)	0.0437	0.0334	0.0394	0.0352	0.0299	0.0227	0.0393
^{12}N$\rightarrow^{12}$C								
1^+1, 0^+0	0.2950(21)	0.3508	0.2467	0.4024	0.3867	0.3228	0.4820	0.5064
1^+1, 2^+0	0.0273(5)	0.0437	0.0334	0.0394	0.0352	0.0299	0.0227	0.0393
^{12}Be$\rightarrow^{12}$B	0.624(3) [38]	1.526	1.305	2.047	2.079	1.349	2.123	1.786
0^+2, 1^+1								
^{13}B$\rightarrow^{13}$C								
$\frac{3}{2}-\frac{3}{2}$, $\frac{1}{2}-\frac{1}{2}$	0.3580(50)	0.5249	0.4371	0.5744	0.5651	0.4999	0.6523	0.6190
$\frac{3}{2}-\frac{3}{2}$, $\frac{3}{2}-\frac{1}{2}$	0.137(15)	0.1059	0.0763	0.2325	0.2479	0.2071	0.2469	0.1391
$\frac{3}{2}-\frac{3}{2}$, $\frac{5}{2}-\frac{1}{2}$	0.0181(43)	0.0060	0.0022	0.0176	0.0167	0.0122	0.0023	0.0135
^{13}O$\rightarrow^{13}$N								
$\frac{3}{2}-\frac{3}{2}$, $\frac{1}{2}-\frac{1}{2}$	0.3221(83)	0.5249	0.4371	0.5744	0.5651	0.4999	0.6523	0.6190
$\frac{3}{2}-\frac{3}{2}$, $\frac{3}{2}-\frac{1}{2}$	0.110(26)	0.1059	0.0763	0.2325	0.2479	0.2071	0.2469	0.1391
$\frac{3}{2}-\frac{3}{2}$, $\frac{5}{2}-\frac{1}{2}$	0.0106(71)	0.0060	0.0022	0.0176	0.0167	0.0122	0.0023	0.0135
^{13}N$\rightarrow^{13}$C	0.1960(38)	0.2817	0.2218	0.2681	0.2702	0.2109	0.2403	0.2484
$\frac{1}{2}-\frac{1}{2}$, $\frac{1}{2}-\frac{1}{2}$								
^{14}B$\rightarrow^{14}$C								
2^-2, 1^-1	0.291(40)	0.3124	0.2695	0.3752	0.3598	0.3273	0.3060	0.3257
2^-2, 3^-1	0.038(2)	0.0517	0.0338	0.0571	0.0523	0.0399	0.0646	0.0350
^{14}C$\rightarrow^{14}$N								
0^+1, 1^+0	$0.346(3)\times10^{-6}$	0.02259	0.00831	0.00922	0.00329	0.533×10^{-4}	0.00651	0.0175

TABLE I. (*Continued*).

Transition $J_i^\pi T_i$, $J_f^\pi T_f$	Experiment	PSDMK2		OFU*	Present		PSDWBP	PSDWBT
$^{14}O \rightarrow {}^{14}N$								
0^+1, 1^+0	$0.202(4)\times10^{-6}$	0.02259	0.00831	0.00920	0.00329	0.534×10^{-4}	0.00651	0.0175
0^+1, 1^+0	2.818(106)	4.803	4.640	4.579	4.577	4.448	4.539	4.445
$^{15}C \rightarrow {}^{15}N$								
$\frac{1}{2}+\frac{3}{2}$, $\frac{1}{2}+\frac{1}{2}$	0.2978(42)	0.3440	0.2381	0.3468	0.3679	0.2297	0.2919	0.4552
$\frac{1}{2}+\frac{3}{2}$, $\frac{3}{2}+\frac{1}{2}$	$0.491(56)\times10^{-3}$	0.0103	0.433×10^{-2}	0.700×10^{-2}	0.547×10^{-2}	0.273×10^{-2}	0.843×10^{-4}	0.521×10^{-2}
$^{15}O \rightarrow {}^{15}N$	0.2490(20)	0.3333	0.3172	0.3333	0.3333	0.3202	0.3333	0.3333
$\frac{1}{2}-\frac{1}{2}$, $\frac{1}{2}-\frac{1}{2}$								

netic moment of the ground state of ^{12}N was discussed in the preceding section, with a naive estimate $\mu=-0.12\mu_N$. We have seen in Fig. 10 that the present Hamiltonian combined with the corrected $g_\pi^{(\ell)}$'s can reproduce the experimental value, $0.46\mu_N$.

A similar situation occurs in ^{12}B. The same naive estimate gives us $\mu=g_\pi^{(\ell)}+\frac{1}{2}(g_\pi^{(s)}+g_\nu^{(s)})=1.88\mu_N$. This is much too large as compared to the experimental value $1.00\mu_N$. The CK Hamiltonian, however, drives down the moment excessively to $0.60\mu_N$ due to too strong mixing between $0p_{3/2}$ and $0p_{1/2}$. In fact, the CK (or PSDMK2) changes the magnetic moments of ^{12}B and ^{12}N too much by the mixing, the resultant values show $\mu(^{12}B)<\mu(^{12}N)$, whereas experimentally the relation is opposite. The present Hamiltonian produces values close to experiment, because of weaker mixing, and satisfies the relation $\mu(^{12}B)>\mu(^{12}N)$.

TABLE II. Calculated and observed values of magnetic moments in *p*-shell nuclei in the unit of μ_N. Calculated values are obtained within $(2–3)\hbar\omega$ space except for the CK, and OFU* and PSDWBP Hamiltonians, where the configuration space is restricted to $0\sim1\hbar\omega$ excitations. In the column CK, values marked with an asterisk are actually obtained by using the PSDMK2 Hamiltonian in the $(0–1)\hbar\omega$ space instead of CK (8–16). The label IV denotes that the mesonic correction to the isovector orbital *g* factor is included.

Nucleus	Experiment	CK	PSDMK2	OFU*-IV	Present	Present-IV	PSDWBP-IV
^{7}Li	3.2564286(17)	3.235	3.236	3.253	3.232	3.247	3.150
^{8}Li	1.65356(18)	1.377	1.386	1.687	1.759	1.691	1.226
^{8}B	1.0355(3)	1.298	1.282	0.912	0.839	0.907	1.460
^{9}Li	3.4391(6)	3.471	3.446	3.552	3.423	3.533	3.660
^{9}Be	−1.1778(9)	−1.288	−1.277	−1.169	−1.081	−1.172	−1.451
^{9}B		3.109	3.098	2.946	2.859	2.949	3.276
^{9}C	−1.3914(5)	−1.585	−1.566	−1.640	−1.514	−1.625	−1.768
^{10}B	1.8006448(6)	1.811	1.813	1.811	1.814	1.814	1.828
^{10}B (1^+)	0.63(12)	0.778	0.815	0.786	0.810	0.810	0.793
^{11}Li	3.6678(25)	3.793	3.715	3.943	3.549	3.658	3.943
^{11}Be	−1.6816(8)	−1.705*	−1.740	−1.666	−1.632	−1.661	−1.562
^{11}B	2.6886489(10)	2.534	2.480	2.739	2.614	2.7175	3.012
^{11}C	−0.964(1)	−0.806	−0.753	−1.000	−0.871	−0.975	−1.238
^{12}B	1.00306(15)	0.599	0.399	1.073	0.741	0.929	1.122
^{12}N	0.4573(5)	0.778	0.976	0.310	0.641	0.452	0.248
^{13}B	3.1778(5)	3.097	3.008	3.270	3.032	3.194	3.326
^{13}C	0.7024118(14)	0.700	0.755	0.591	0.707	0.646	0.532
^{13}N	−0.3222(4)	−0.334	−0.385	−0.227	−0.340	−0.278	−0.173
^{13}O	−1.3891(3)	−1.333	−1.251	−1.505	−1.271	−1.434	−1.552
^{14}B	1.185(5)	0.997*	0.989	1.111	1.014	1.117	0.898
^{14}N	0.403761	0.326	0.327	0.327	0.329	0.329	0.334
^{15}B	2.659(15)	2.596*	2.585	2.669	2.577	2.669	2.935
^{15}C	−1.720(9)	−1.804*	−1.785	−1.800	−1.769	−1.776	−1.9147
^{15}N	−0.28318884(5)	−0.264	−0.279	−0.164	−0.278	−0.186	−0.164
^{15}O	0.7189(8)	0.638	0.652	0.538	0.650	0.559	0.538

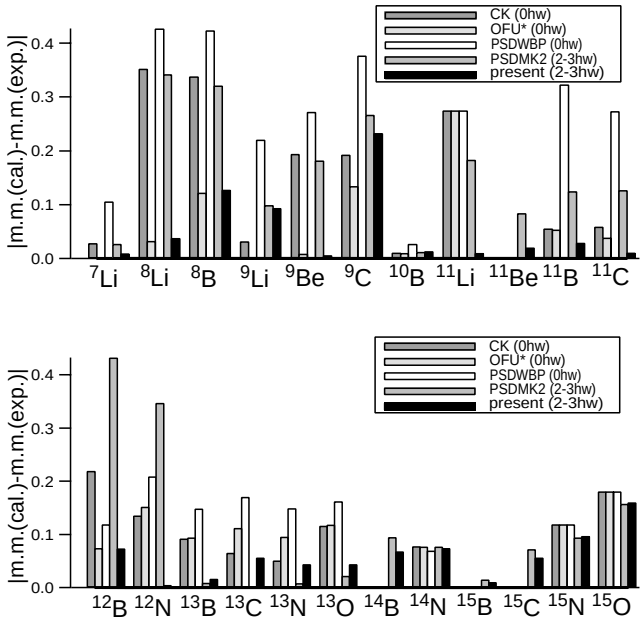

FIG. 11. Deviations of calculated magnetic moments from experimental ones for *p*-shell nuclei with five Hamiltonians as indicated in the figure. Here, the isovector mesonic correction to the orbital *g* factor, $\delta g_\ell^{IV}=0.15$, is used in all calculations.

We next briefly discuss the ^{11}B-^{11}C mirror pair. The $0p_{1/2}$ occupation number becomes smaller by the present Hamiltonian than that by the PSDMK2, due to a weaker mixing between $0p_{1/2}$ and $0p_{3/2}$. This leads to slightly larger magnitude of the magnetic moment for the present Hamiltonian in both ^{11}B and ^{11}C. This is also the case with ^{13}B-^{13}O mirror pair, though the difference is rather small.

For pairs of mirror nuclei such as ^{8}Li-^{8}B, ^{11}B-^{11}C, and ^{12}B-^{12}N, the isovector part of the magnetic moments becomes closer to experiment by the modification of the Hamiltonians, while the isoscalar part is not affected so much, as can be seen in Table II. Those are mirror pairs with higher isospin, and should be more sensitive to the change of the spin-isospin component of the Hamiltonian.

Magnetic moments of unstable nuclei recently measured, ^{14}B and ^{15}B [39], are also well described by the OFU* and present Hamiltonians (see Table II).

Finally, we show in Fig. 11 the deviations of the calculated magnetic moments from the experimental ones. We notice that the present Hamiltonian results in the smallest deviations in most of the *p*-shell nuclei, especially for those with smaller mass numbers. In this study, the spin *g* factors are kept unchanged. In Ref. [40], meson exchange current (MEC) effects were studied in *p*-shell nuclei in $(0-2)\hbar\omega$ configuration space. The MEC contributions were found to improve the agreement between the calculation and observed values. The effects can also be simulated by renormalized spin and orbital *g* factors. Fitting by parametrization without MEC in *p*-shell nuclei in $(0-2)\hbar\omega$ space leads to $\delta g_\ell^{IV}\sim 0.22$ and $\delta g_s^{IV}\sim 0.55$ ($\delta g_S^{IV}/g_S^{IV}=0.12$) for isovector *g* factors and $\delta g_\ell^{IS}\approx \delta g_S^{IS}\sim 0$ for isoscalar ones [40]. This result seems to support the use of $\delta g_\ell^{IV}=0.15$ without quenching of g_s in the present calculation.

The quenching of spin *g* factors [5,6] can have some effects on the value of magnetic moments. The coupling to higher than $(2-3)\hbar\omega$ configurations quenches the spin *g* factors, while the MEC enhances it. Although there are several contributions to δg_s and they may vary from nucleus to nucleus, a single value of g_s^{eff}/g_s is taken for all *p*-shell nuclei, for simplicity. We take $g_s^{eff}/g_s=0.95$ for the isovector spin *g* factor, as the same value, $g_A^{eff}/g_A=0.95$, was obtained in Sec. III by fitting the $B(GT)$ value in ^{12}C to experiment. Effects of the change of g_s^{IV} are found to be rather small in $A=7-14$ system. The root mean square deviation of the calculated magnetic moments from the experimental ones remain almost unchanged in $A=7-14$ system, that is, $0.080\mu_N$ for $\delta g_s^{IV}=0$ in the present-IV case and $0.083\mu_N$ for $g_{s,eff}^{IV}/g_s^{IV}=0.95$.

Effects of $\delta g_p[Y_2\times\vec{s}]^1$ term on the magnetic moments can be significant in some nuclei such as ^{15}N, ^{15}O, ^{13}N, and ^{13}C, where the $0p_{1/2}$-$0p_{1/2}$ transition is dominant. The effects can be as large as 16–45 % of the experimental values for $\delta g_p^{IV}=1.0$ [5,6] for the isovector term. In some other nuclei such as ^{8}B, ^{11}C, ^{12}N, ^{13}O, and ^{15}B, the effects are smaller but not negligible, as large as 4–7 % of the experimental values. In most of these nuclei, inclusion of both g_s^{eff} and δg_p in isovector *g* factors improves the agreement with experiments, especially in $A=15$ and 13 systems. The deviation of the calculated value from the observed one becomes as small as $0.009\mu_N$ in ^{15}N, $-0.072\mu_N$ in ^{15}O, $0.018\mu_N$ in ^{13}C, $-0.031\mu_N$ in ^{13}N, and $-0.020\mu_N$ in ^{13}O. The deviation is found to remain as small as $-0.0134\mu_N$ for ^{12}N. The effects of the δg_p term are smaller and insignificant for other *p*-shell nuclei. The root mean square deviation for $A=7-14$ systems becomes a smaller value of $0.077\mu_N$ for $g_{s,eff}^{IV}/g_s=0.95$ and $\delta g_p^{IV}=1.0$. The deviation is diminished to $-0.164\mu_N$ in ^{9}C, the largest case in Fig. 11. The effect of δg_p^{IV} on a magnetic dipole transition, $^{12}\mathrm{C}_{\mathrm{g.s.}}\rightarrow{}^{12}$C ($1^+$, $T=1$, 15.1 MeV), for example, is found to be insignificant. Calculated $B(M1)$ values are $2.426\mu_N^2$ and $2.515\mu_N^2$ with and without the $g_p^{IV}=1.0$ term, respectively. Here, bare spin and orbital *g* factors are used. These values can be compared with the experimental value of $(2.897\pm 0.060)\mu_N^2$ [35]. The discrepancy can be explained by the MEC current effects that enhance the $B(M1)$ value by about 15% [29].

From an overall inspection, one notices that the major deviations remain in ^{8}B and ^{9}C [41]. Both are well known with their small proton separation energies, and it is likely that such loose binding changes their magnetic moments. This issue is beyond the present study where the focus is on the role of the effective nucleon-nucleon interaction. The issue of loose binding should be studied in the future. It is of interest that one can pick up such special cases in this systematic comparison.

Other notable deviations are found towards the heavy end of the figure, though some part can be remedied by the inclusion of the δg_p^{IV} term just discussed above. This is natural because couplings with *sd*-shell configurations should become more important in this direction, but the *sd*-shell part of the Hamiltonian remains untouched so far. This is another

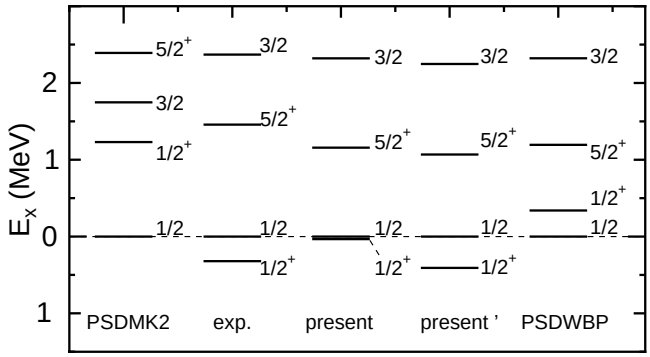

FIG. 12. Comparison of calculated and experimental energy levels for ^{11}Be. Calculated energy levels are obtained for the PSDMK2, and for the present and the PSDWBP Hamiltonians. For the present′ Hamiltonian, see the text in Sec. VIII.

important future problem, which will be touched upon briefly in Sec. VIII.

VII. STRUCTURE AND MAGNETIC MOMENT OF ^{11}Be

We show in Fig. 12 calculated energy levels of ^{11}Be in comparison to experimental ones. As emphasized in Ref. [2], the modification of the Hamiltonian in terms of $\Delta\varepsilon_p$ in Eq. (2) and $V_M^{T=0}$ in Eq. (1) enables us to describe the anomalous ground state of ^{11}Be correctly within the same framework as for other stable and exotic nuclei. The results in Fig. 12 are obtained in the $2\hbar\omega$ space, whereas those reported in Ref. [2] were obtained in the $0\hbar\omega$ space. The same mechanism determines level structure in both cases, though.

We here discuss the magnetic moment of ^{11}Be. Calculated values are shown in Fig. 13. The observed value [42] is close to those obtained by the OFU* Hamiltonian in the $1\hbar\omega$ space and present Hamiltonian in the $3\hbar\omega$ space. The occupation probability of the $1s_{1/2}$ orbit, which is primarily coupled to the ^{10}Be (0^+) core state in the ^{11}Be wave function, is 73–74 % for the Hamiltonians used here. These values can be compared to the observed spectroscopic factors 73–77 % [43] and 84% [44].

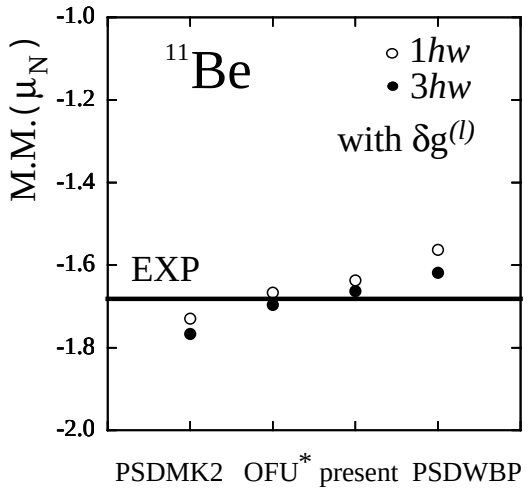

FIG. 13. The same as in Fig. 10 for the magnetic moment of ^{11}Be. Experimental value is taken from Ref. [42].

VIII. $N=8$ ISOTONES ^{11}Li AND ^{12}Be

Finally, we comment on nuclei with $N=8$ near the neutron drip line: ^{11}Li and ^{12}Be. In these nuclei, due to the small Z, the proton $p_{3/2}$ is rather vacant, and the neutron $p_{1/2}$ is not pulled strongly down by the $j_>$-$j_<$ p-n monopole interaction, and stays rather high. This makes the gap between $0p_{1/2}$ and $1s_{1/2}$ for the neutrons smaller. Due to this smaller gap and occupations up to $N=8$, more excitations to the sd shell are likely to occur in ^{11}Li and ^{12}Be. Thus, for these two nuclei, the interaction must be well tuned for the sd-shell sector too. We will not address such an issue fully in the present paper. Here, a rather simple attempt is taken. As a minimal improvement from the present Hamiltonian, we introduce two simple modifications. (1) The single-particle energies of the sd shell should be lowered by 0.3–0.5 MeV, (2) the pairing matrix element $\langle 0p_{1/2}^2, J=0, T=1|V|1s_{1/2}^2, J=0, T=1\rangle$ is increased to 1.0 MeV. Note that this value of pairing is reasonable in terms of global systematics, but is stronger than the PSDMK2 value. First of all, by these changes related to the sd shell, the descriptions of p-shell nuclei with $N\leqslant 7$ are not changed much. For instance, the magnetic moment of ^{12}B (^{12}N) is changed, from its present-IV value of $0.929\mu_N$ $(0.452\mu_N)$ to $0.918\mu_N$ $(0.464\mu_N)$.

Note that the modifications made in Sec. II are all for the p-shell part, and contain no changes for parts involving sd-shell orbits. The Hamiltonian containing the above changes (1) and (2) will be referred to as the present′ Hamiltonian.

In case of the PSDMK2 Hamiltonian, a large modification of the single-particle energies of the sd shell, as large as -3 MeV, was necessary to bring about sufficient admixture of the sd-shell components [18,19]. This is simply because the neutron $p_{1/2}$ is effectively much lower in ^{11}Li and ^{12}Be in the PSDMK2.

The total probability of pure p-shell components in the ground state is 39% (44%) for ^{11}Li (^{12}Be) with the present′ Hamiltonian, whereas it is 60% (59%) with the present Hamiltonian. The $B(GT)$ value for ^{12}Be thus obtained is 1.016 compared with the value of 1.349 for the present Hamiltonian, indicating certain improvement in the agreement to experiment.

The $B(GT)$ (log ft) value for ^{11}Li in the same calculation is 0.0412 (4.973), which is still far from the experimental value in Table I, which is the averaged one for the three values 0.010 12(85) [12], 0.008 31(81) [13], and 0.007 24(50) [14]. On the other side, ^{11}Li has a well-developed neutron halo, and we shall take into account its effects on GT transitions in a simple manner. By using a Woods-Saxon potential, the $1s_{1/2}$ radial wave function is generated by adjusting the potential depth so that the energy eigenvalue is -160 keV, which is adopted from the average observed $S_{2n}=320$ keV [45]. The potential radius and diffuseness are assumed to be 2.5 fm and 0.65 fm, respectively. These are within the range of usual values. Note that this

wave function at this energy region is not very sensitive to these parameters anyway. The rms radius of $1s_{1/2}$ turns out to be about 10.6 fm, which is the major source of the neutron halo of ^{11}Li. Our shell-model calculation indicates that the mixing probabilities are about 1/2, 1/4, and 1/4, respectively, for the $(0p_{1/2})^2$, $(1s_{1/2})^2$, and $(0d_{5/2})^2$ configurations of the last two neutrons. The radial wave functions of $0p_{1/2}$ and $0d_{5/2}$ are calculated similarly. The rms radius of the last neutron of ^{11}Li then becomes 7.1 fm, which can be compared to a recent experimental estimate, 6.54 ± 0.38 fm [46]. By using these single-particle wave functions with slowly damping tails, the $B(GT)$ value is calculated as 0.009 49, as compared to the above-mentioned averaged value of experimental data: 0.0086(24) [12–14]. This analysis is a quite simple one, but already suggests how much GT transitions can be further retarded by loose binding: $B(GT)$ is reduced by 77%. We also note that this is probably the maximum change of $B(GT)$ due to neutron halo.

The above modifications of the sd-shell single particle energies and the pairing interaction induce rather small changes in calculated magnetic moments, as small as about 1%. The exception is ^{11}Li, where the gap between $0p_{1/2}$ and $1s_{1/2}$ is smallest among the cases considered, and moreover, $N=8$ means the highest sensitivities to such modifications. Due to this subtleness, the present′ Hamiltonian actually gives us a somewhat larger deviation from the observed magnetic moment, $0.10\mu_N$. The modifications (1) and (2) mentioned above for creating the present′ Hamiltonian have opposite effects on the magnetic moment.

The contamination of spurious states is eliminated by the method of Ref. [47], while it is monitered in terms of the expectation value of the harmonic oscillator quanta (without the zero-point oscillation contribution) of the center-of-mass motion. This value should be vanished for a spurious free state, and it turns out to be, for instance, 0.000 03, 0.000 02, and 0.000 03, respectively, for ^{12}N (ground state), ^{11}Li (ground state), and ^{14}C (first 1^- state) with the most relevant Hamiltonians. Thus, the mixing probability of the spurious states is quite small. On the other hand, when the space is extended to the complete $1\hbar\omega$ space of $0s$-$0p$-$1s0d$ configuration, the spurious states can be separated completely. In this case, the Hamiltonian is changed and hence all the physical observables can be changed. A shell-model Hamiltonian is constructed associated with a particular model space, and the tune-up of the Hamiltonian is more difficult in the complete space due to higher complexity than in a more restricted space. In the case of ^{11}Be discussed in the preceding section, the magnetic moment calculated by the WBP (WBT) [22] Hamiltonian in the $0s$-$0p$-$1s0d$ configuration space turns out to be $-1.492\mu_N$ ($-1.512\mu_N$), which differs more from the experimental value as compared to the PSD-WBP (PSDWBT) value of $-1.523\mu_N$ ($-1.595\mu_N$). Nevertheless, it may be of much interest to derive a complete-space Hamiltonian in a way consistent to the present Hamiltonian.

At the end, we discuss the energy levels and $E2$ transitions of ^{12}Be. Calculated energy levels of ^{12}Be are shown in Fig. 14 as well as the experimental ones [48]. The second 0^+ level is obtained around $E_x=2.2$ MeV, which is close to the recent observed value of $E_x=2.2$ MeV [48]. The other low-lying levels are reproduced similarly well. Because of strong excitations from the p to the sd shells, the configuration space is taken up to $4\hbar\omega$. The sd-shell part of the 0_1^+ and 0_2^+ wave functions are of pairing type, with strong mixing of the $\nu(1s_{1/2})^2$ component. The p-shell wave function $\nu(0p_{1/2})^2$ is its major mixing partner. Relative mixing amplitudes between the $\nu(1s_{1/2})^2$ and $\nu(0p_{1/2})^2$ components change sign between the first and second 0^+ states. The second 0^+ level is raised to around 3.6 MeV for the PSDMK2 Hamiltonian, since the $1s_{1/2}-0p_{1/2}$ effective gap is much wider. In this case, the 0_1^+ and 0_2^+ states are of nearly pure $0\hbar\omega$ and $2\hbar\omega$ configurations, respectively. Furthermore, the spacing between these two states shows certain sensitivity to the pairing matrix elements of the $0p_{1/2}$ and $1s_{1/2}$ orbits, and therefore the present result may suggest the range of the strength. Without the above modification of the pairing matrix element, the 0_2^+ state comes down as low as 1.4 MeV. The $B(E2;0_2^+\rightarrow2_1^+)$ value is calculated to be $28.0e^2$ fm^4 (17.1 W.u.) with the use of the effective charges of $e_p=1.5$ and $e_n=0.5$. This $B(E2)$ value corresponds to the decay rate of 1.8×10^6 sec^{-1}. This $B(E2)$ value is much enhanced compared to the one for the PSDMK2; $0.57e^2$ fm^4 (0.35 W.u.). As the experimental branching ratio of the $E2$ transition is about 17% [48], the mean lifetime of the 0_2^+ state is estimated to be about 100 ns. This falls within the experimental range of the mean lifetime for the 0_2^+ state between 50 ns and 10 μs [48].

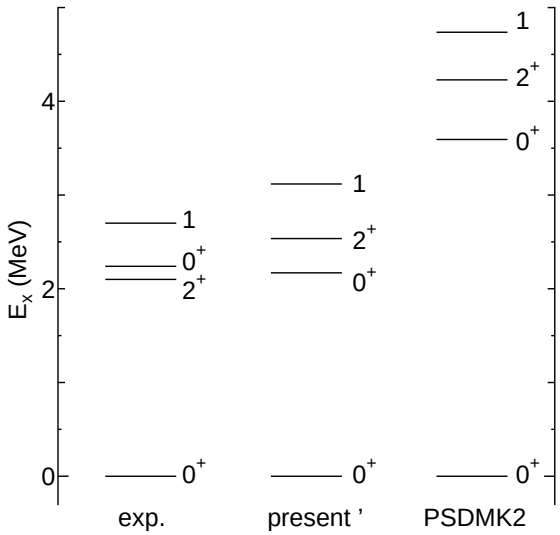

FIG. 14. Calculated energy levels of ^{12}Be as well as the experimental ones.

It is of interest what levels the present′ Hamiltonian produces for ^{11}Be. Figure 12 includes such results, where one finds that the intruder $1/2^+$ ground state is better reproduced with a wider spacing to the $1/2^-$ excited state. This suggests that the present′ Hamiltonian is on the right track, but a more elaborate systematic study is needed to find out a reliable shell-model Hamiltonian for heavier $p+sd$ nuclei.

IX. SUMMARY

In summary, we have made a systematic shell-model study over *p*-shell nuclei, stable and unstable. A modified Hamiltonian that properly takes into account an important role of the $j_>$-$j_<$ *p*-*n* monopole interaction was introduced, as referred to as the present Hamiltonian. The calculations were carried out in the $p+sd$ space up to $(2-3)\hbar\omega$ excitations from the *p* shell. The present Hamiltonian is an improved version of a similar but original Hamiltonian, OFU* [2], used in the $(0-1)\hbar\omega$ shell-model space to illustrate basic physics. By having the $(2-3)\hbar\omega$ space, we can use bare parameters for magnetic and GT properties. We thus investigate GT transitions and magnetic moments for a large fraction of *p*-shell nuclei. It has been proven that the present Hamiltonian can explain the strength of GT transitions in $^{12}\mathrm{C}\rightarrow{}^{12}\mathrm{N}$, $^{11}\mathrm{B}\rightarrow{}^{11}\mathrm{Be}$, and $^{9}\mathrm{Li}\rightarrow{}^{9}\mathrm{Be}$, where the quenching varies and is weaker especially in the second case. This is due to the variation of the effective $0p_{3/2}$-$0p_{1/2}$ spacing, as a result of the shell evolution originated from the $j_>$-$j_<$ *p*-*n* monopole interaction. The magnetic moment is studied by the same Hamiltonian with considerable improvements in the agreement to experimental data, for which the example of $^{12}\mathrm{N}$ was explained. The systematic comparison indicates that the agreement of calculated $B(GT)$ values and magnetic moments with experimental values is generally improved in most of the *p*-shell nuclei investigated here, especially in lighter nuclei. We stress once more that the degree of quenching of the spin-isospin properties does depend on occupations of individual orbits, and final $B(GT)$ and magnetic moments can vary considerably, in particular in nuclei far from stability. We notice that the isovector correction due to mesonic effects plays an important role in orbital *g* factors systematically, and this aspect can be strengthened in exotic nuclei because of higher isospin. We also note that, with the present Hamiltonian, we can explain branching ratios of proton emission after GT transitions in $^{13}\mathrm{C}\rightarrow{}^{13}\mathrm{N}$ [49] better than with the CK.

Thus, we can confirm that the modification of the Hamiltonian required for the description of the structure of exotic nuclei has a general and different aspect that can improve spin-isospin properties of nuclei such as GT transitions and magnetic moments. Since the modification has been proposed in the line of the paradigm of shell evolution, the present study provides us with another strong support to this paradigm [2,3]. While this paradigm is about important and specific roles of certain monopole interaction, the general importance of the monopole interaction has been emphasized by Poves and Zuker [50], and is now reinforced by the present study.

ACKNOWLEDGMENTS

The authors would like to thank Professor H. Sakai, Dr. T. Onishi, Professor M. Ishihara, and Professor K. Asahi for valuable discussions on their experiments. The authors acknowledge Professor A. Gelberg for a careful reading of the manuscript. One of them (T.S.) is grateful to Professor J. P. Deutsch and Professor K. Riisager for their interest in our work of the muon-capture reaction. This work was a part of the CNS-RIKEN joint research project on nuclear shell model. The shell-model calculations were made by the codes OXBASH [22] and MSHELL [51]. This work was supported in part by a Grant-in-Aid for specially promoted research (Grant No. 13002001) from the Ministry of Education, Culture, Sports, Science and Technology, and in part by a Grant-in-Aid to promote advanced scientific research from the same ministry. One of the authors (R.F.) acknowledges partial support of the Japan Society for the Promotion of Science for Young Scientists.

[1] M.G. Mayer, Phys. Rev. **75**, 1969 (1949); O. Haxel, J.H.D. Jensen, and H.E. Suess, *ibid.* **75**, 1766 (1949).
[2] T. Otsuka, R. Fujimoto, Y. Utsuno, B.A. Brown, M. Honma, and T. Mizusaki, Phys. Rev. Lett. **87**, 082502 (2001).
[3] T. Otsuka, Prog. Theor. Phys. Suppl. **146**, 6 (2002).
[4] M. Hjorth-Jensen, T.T.S. Kuo, and E. Osnes, Phys. Rep. **261**, 125 (1995); M. Hjorth-Jensen (private communication).
[5] A. Arima, K. Shimizu, W. Bentz, and H. Hyuga, Adv. Nucl. Phys. **18**, 1 (1986); A. Arima and H. Hyuga, in *Mesons in Nuclei*, edited by D.H. Wilkinson and M. Rho (North-Holland, Amsterdam, 1979), Vol. II, p. 683.
[6] I.S. Towner, Phys. Rep. **155**, 263 (1987); I.S. Towner and F.C. Khanna, Nucl. Phys. **A399**, 334 (1983).
[7] S. Cohen and D. Kurath, Nucl. Phys. **73**, 1 (1965).
[8] B.A. Brown and B.H. Wildenthal, Annu. Rev. Nucl. Part. Sci. **38**, 29 (1988).
[9] P. Raghavan, At. Data Nucl. Data Tables **42**, 189 (1989).
[10] R.E. McDonald, J.A. Becker, R.A. Chalmers, and D.H. Wilkinson, Phys. Rev. C **10**, 333 (1974).
[11] T. Ohnishi *et al.*, Nucl. Phys. **A687**, 38c (2001).
[12] E. Roeckl, D.F. Dittner, C. Detraz, R. Klapisch, C. Thibault, and C. Rigaud, Phys. Rev. C **10**, 1181 (1974).
[13] N. Aoi *et al.*, Nucl. Phys. **A616**, 181c (1997).
[14] M.J.G. Borge *et al.*, Phys. Rev. C **55**, R8 (1997).
[15] N. Kumar, Nucl. Phys. **A225**, 221 (1974).
[16] L. Coraggio, A. Covello, A. Gargano, N. Itaco, and T.T.S. Kuo, J. Phys. G **27**, 2351 (2001).
[17] T. Suzuki and T. Otsuka, Phys. Rev. C **50**, R555 (1994).
[18] T. Suzuki and T. Otsuka, Phys. Rev. C **56**, 847 (1997).
[19] T. Suzuki and T. Otsuka, Nucl. Phys. **A635**, 86 (1998).
[20] D.J. Millener and D. Kurath, Nucl. Phys. **A255**, 315 (1975).
[21] T.T.S. Kuo, Nucl. Phys. **A103**, 71 (1967).
[22] OXBASH, the Oxford, Buenos-Aires, Michigan State, Shell Model Program, B.A. Brown, A. Etchegoyan, and W.D.M. Rae, MSU Cyclotron Laboratory Report No. 524, 1986.
[23] T. Sebe *et al.* (unpublished).
[24] J.C. Hardy, I.S. Towner, V.T. Koslowsky, E. Hagberg, and H. Schmeing, Nucl. Phys. **A509**, 429 (1990).
[25] P. Bopp, D. Dubbers, L. Hornig, E. Klemt, J. Last, H. Schütze, S.J. Freedman, and O. Schärpf, Phys. Rev. Lett. **56**, 919 (1986); D. Dubbers, Nucl. Phys. **A527**, 239c (1991).
[26] E.K. Warburton and B.A. Brown, Phys. Rev. C **46**, 923 (1992).

[27] A.C. Hayes, Phys. Rep. **315**, 257 (1999); D.J. Millener, Nucl. Phys. **A693**, 394 (2001).
[28] K. Yoro, Nucl. Phys. **A333**, 67 (1980).
[29] T. Suzuki, H. Hyuga, A. Arima, and K. Yazaki, Phys. Lett. **106B**, 19 (1981).
[30] V.V. Balashov and R.A. Eramzhyan, At. Energy Rev. **5**, 3 (1967); M. Morita and A. Fujii, Phys. Rev. **118**, 606 (1960).
[31] T. Suzuki, in *Proceedings of the International Symposium on Non-Nucleonic Degrees of Freedom Detected in Nuclei, Osaka, 1996*, edited by T. Minamisono *et al.* (World Scientific, Singapore, 1997), p. 349.
[32] J.P. Deutsch *et al.*, Phys. Lett. **28B**, 178 (1968).
[33] R. Prieels, in *Proceedings of the 14th International Conference on Particles and Nuclei (PANIC '96)*, edited by C.E. Carlson and J.J. Domingo (World Scientific, Singapore, 1997), p. 568.
[34] G. Nyman *et al.*, Nucl. Phys. **A510**, 189 (1990).
[35] F. Ajzenberg-Selove, Nucl. Phys. **A523**, 1 (1991); **A490**, 1 (1988); **A449**, 1 (1986); **A336**, 1 (1980).
[36] *Table of Isotopes*, edited by R.B. Firestone *et al.* (Wiley, New York, 1996).
[37] W.-T. Chou, E.K. Warburton, and B.A. Brown, Phys. Rev. C **47**, 163 (1993).
[38] U.C. Bergmann *et al.*, Nucl. Phys. **A658**, 129 (1999).
[39] H. Okuno *et al.*, Phys. Lett. B **354**, 41 (1995).
[40] J.G.L. Booten, A.G.M. van Hees, P.W. Glaudemans, and R. Wervelman, Phys. Rev. C **43**, 335 (1991).
[41] K. Matsuta *et al.*, Nucl. Phys. **A588**, 153c (1995).
[42] W. Geithner *et al.*, Phys. Rev. Lett. **83**, 3792 (1999).
[43] D.L. Auton, Nucl. Phys. **A157**, 305 (1970); B. Zweiglinski, W. Benenson, and R.G.H. Robertson, *ibid.* **A315**, 124 (1979).
[44] S. Fortier *et al.*, Phys. Lett. B **461**, 22 (1999).
[45] T. Kobayashi, in *Proceedings of the International Symposium on Structure and Reactions of Unstable Nuclei*, edited by K. Ikeda and Y. Suzuki (World Scientific, Singapore, 1991), p. 187; B.M. Young *et al.*, Phys. Rev. Lett. **71**, 4124 (1993).
[46] P. Egelhof, Prog. Part. Nucl. Phys. **46**, 307 (2001).
[47] D.H. Gloeckner and R.D. Lawson, Phys. Lett. **53B**, 313 (1974).
[48] S. Shimoura *et al.* (private communication).
[49] M. Fujimura *et al.*, Ph.D. thesis, Osaka University, Osaka, 2002; (private communication).
[50] A. Poves and A. Zuker, Phys. Rep. **70**, 235 (1981).
[51] T. Mizusaki, RIKEN Accel. Prog. Rep. **33**, 14 (2000).
[52] Values in Fig. 5 are those with the renormalization effects while the shaded histogram in Fig. 4 is obtained without them.